Basic single-event mechanisms in Ge-based nanoelectronics subjected to terrestrial atmospheric neutrons

Daniela Munteanu, Soilihi Moindjie, Jean-Luc Autran

Basic single-event mechanisms in Ge-based nanoelectronics subjected to terrestrial atmospheric neutrons

D. Munteanu, S. Moindjie, J.L. Autran*

Aix-Marseille University & CNRS, IM2NP (UMR 7334), Faculté des Sciences – Service 142, Avenue Escadrille Normandie Niémen, F-13397 Marseille Cedex 20, France

Abstract

Germanium is potentially candidate to replace silicon in ultra-scaled transistors. This work analyses the radiation response of germanium in thin layer subjected to atmospheric neutrons simulated with Geant4 and quantifies the underlying mechanisms potentially responsible of single event effects in Ge-based CMOS technologies. From this analysis of interactions at material-level, reliability assessments for Ge-based nanoelectronics are tentatively deduced for technological nodes ranging from 180 nm to 5 nm in terms of nature and number of nuclear events susceptible to upset a SRAM memory cell. Finally, first soft error rate projections are performed for germanium SRAMs in 130, 65 and 40 nm based on a simulation methodology previously developed and fully validated on silicon memories also characterized by real-time experiments.

Keywords

Germanium, single events, atmospheric neutrons, neutron interactions, Geant4, radiation transport, CMOS technological node, SRAM, critical charge, single event upset

Highlights

- Interactions of atmospheric neutrons with germanium thin film materials is investigated using Geant4 simulations
- Secondaries produced in Ge material are characterized in terms of energy, linear energy transfer and range distributions
- Low energy recoils are much more important in Ge than in Si, doubling the number of products between 180 and 5 nm nodes
- SER values of Ge-SRAMs at 130, 65 and 40 nm are found in the same order of magnitude than the ones related to Si-SRAMs.

* **Corresponding author:**
Prof. Jean-Luc Autran, IM2NP - UMR CNRS 7334**,** Faculté des Sciences – Service 142**,** Avenue Escadrille Normandie **–** F-13397 Marseille Cedex 20 France – Phone: + 33 (0)413 594 627 – Email: jean-luc.autran@univ-amu.fr

1. Introduction

Germanium was the semiconductor material of first-generation transistors in the late 1940s and early 1950s before it was replaced by silicon for large scale-area microelectronics [1]. However, using germanium instead of silicon as transistor material would enable more performant transistors and faster chips because of its higher mobility values for electrons and holes than those of silicon. In the last years, significant progress in passivation of the interface between Ge material and high-k gate dielectrics has revived the interest of Ge for ultra-scaled devices as a potential candidate for high-mobility channel material [2-10], in particular for nanosheet transistors, the next and maybe ultimate device architecture in Moore's Law for device integration [11]. From a radiation reliability point-of-view, Ge is therefore characterized by a lower energy of electron-hole pair creation than Si, that questions its susceptibility to radiation in general, and to natural radiation at atmospheric level for this study.

Following a robust methodology previously used for the study of neutron interactions with silicon [12-14] and III-V materials [15], this work also extends our study concerning a first estimation of stability of Ge-based SRAMs subjected to single event effects (SEE) [16]. The present contribution precisely examines the susceptibility to atmospheric neutrons of a thin film of natural Ge, mimicking the active semiconductor top layer of a typical integrated circuit. In the following, we report a complete analysis of neutron-Ge interactions in terms of number/types of reactions and number/nature of secondary products produced in Ge and Si targets. We also discuss the impact of the energy of secondaries and its corresponding amount of deposited charge in the semiconductor target with respect to the critical charge of SRAM cells for CMOS technological nodes from 180 nm to 5 nm, suggesting the increasing importance of low energy products in the SEE occurrence probability when pushing the integration. Finally, first soft error rate estimations are performed for germanium SRAMs in bulk 130, 65 and 40 nm following the same methodology previously used to simulate silicon memories also characterized by real-time experiments.

2. Simulation details

We used a recent version of Geant4 (10.06.p01 with G4NDL4.6 neutron library and QGSP_BIC_HP physics list [17]) to numerically simulate the impact of high energy (E>1 MeV) atmospheric neutrons on a thin film ($1 cm^2 \times 20$ µm) of natural Ge (and of natural Si for comparison), following the methodology detailed in Ref. [15]. This simple geometry is representative of the typical "active volume" of a microelectronic circuit. In the present case, we considered the natural isotopic composition of natural Ge, which is a mixture of five isotopes detailed in Table 1 which also summarizes other main physical and electronic properties of both Si and Ge materials. A total of 5×10^8 of incident neutrons (arriving perpendicularly to the target largest surface) has been randomly generated; it corresponds to a theoretical duration of 25×10^6 hours of natural irradiation at sea-level. The atmospheric neutron flux measured by Goldhagen et al. [18] and modeled by Gordon et al. [19] was used as the neutron environment model (particle source) in Geant4.

Table 1. Main properties of natural germanium and silicon at 300 K.

Properties (300 K)	Natural Si	Natural Ge
Atomic number	14	32
Bandgap (eV)	1.124	0.661
Density (g/cm^3)	2.329	5.3267
Atoms (/cm^3)	5.0×10^{22}	4.42×10^{22}
Natural abundance	^{28}Si (92.22%) ^{29}Si (4.68%) ^{30}Si (3.09%)	^{70}Ge (20.52%) ^{72}Ge (27.45%) ^{73}Ge (7.76%) ^{74}Ge (36.52%) ^{76}Ge (7.75%)
Lattice constant (Å)	5.43	5.65
Energy for creation of an electron-hole pair (eV)	3.6	2.9
Electron mobility (cm^2/V/s)	1400	3900
Hole mobility (cm^2/V/s)	450	1900
Dielectric constant (relative)	11.9	16.1
Intrinsic carrier concentration (cm^{-3})	1×10^{10}	2.4×10^{13}

The simulation output file contains all the information related to the neutron interaction events in the target material. For each event, this information includes the nature and the coordinates of the vertex of the interaction, the energy of the incident neutron, the exhaustive list of secondary particles produced during the interaction (excluding n, γ, π^0, e^+, e^- and η particles that are not able to induce detectable SEE), the energy and the emission direction vector for each of these emitted particles. Contrary to our previous works conducted on other materials [12,15], we did not impose any minimum energy threshold for the secondaries recorded in the output file; in other words, this raw file contains all particles produced by the Geant4 code during the simulation run. As we will see in Section 4, fixing a minimum energy threshold mechanically decreased the number of less energetic events and potentially eliminates secondary products that may induce SEEs in the most integrated technologies.

3. Simulation results

Table 2 summarizes the number of nuclear interactions induced by high energy atmospheric neutrons at sea level during 25×10^6 h in a layer of material of 1 cm^2 × 20 µm. We recall here that interactions of neutrons

with atomic nuclei can be divided in two major mechanisms: scattering (elastic, inelastic) and capture (or nonelastic) [20]. In the elastic scattering, the nature of the interacting particles is not modified; the recoil nucleus is then the same as the target nuclei. The inelastic scattering is similar to the elastic scattering except that the impacted target nucleus undergoes an internal rearrangement into an excited state from which it eventually releases radiation. Instead of being scattered, an incident neutron may be absorbed or captured by a target material nucleus. Many reactions are possible and a large variety of particles can be emitted. This type of interaction is also called nonelastic interaction.

Table 2: Number of nuclear interactions induced by high energy (>1 MeV) atmospheric neutrons at sea level during 25×10^6 h in a layer of material of 1 cm^2 × 20 µm. Results are deduced from Geant4 numerical simulations.

Interactions	Natural Ge	Natural Si
Elastic	66,823 (55.4%)	60,576 (70.6%)
Inelastic	26,604 (22.1%)	8,302 (9.7%)
Nonelastic	27,184 (22.5%)	16,884 (19.7%)
Total	120,611	85,742

Table 3: Details of secondaries produced in natural silicon and germanium targets (1cm^2 × 20 µm, 25×10^8 n) by atmospheric neutrons estimated from Geant4 simulations.

Natural Ge		Natural Si	
Ge recoils	102,492	Si recoils	69,871
p + d + t	24,118	p + d + t	21,292
α + ^{3}He + ^{6}He	3,772	α + ^{3}He + ^{6}He	3,495
Other ions (2 < Z < 32)	16,169	Other ions (2 < Z < 14)	15,799
TOTAL	146,551		110,457

Results of Table 2 show that atmospheric neutrons induce much more interactions in germanium than in silicon: 121 versus 86 kilo-events (+39%) for the considered target geometry and neutron flux. Such an increase with respect to silicon is not uniform: it corresponds to only +10% of elastic events but more than 3 times of inelastic events and about +60% of nonelastic events. For this last category, the nature and the distribution of the most numerous nonelastic reactions are also different:

- For silicon, only 6 reactions producing Al and Mg ions in secondaries represent more than the half of the total number of nonelastic reactions, respectively by order of importance in occurrences: ^{28}Si(n,np)^{27}Al, ^{28}Si(n,2np)^{26}Al, ^{28}Si(n,p)^{28}Al, ^{28}Si(n,2n2p)^{25}Mg, ^{28}Si(n,α)^{25}Mg and ^{28}Si(n,2n)^{27}Si.

- For germanium, the 10 first nonelastic reactions in numbers only represent one third of the total number of events; all these reactions give a germanium nuclei with a lighter mass with respect to the initial impacted nucleus. Also by order of importance, these reactions are: ^{74}Ge(n,2n)^{73}Ge, ^{74}Ge(n,3n)^{72}Ge, ^{72}Ge(n,2n)^{71}Ge, ^{72}Ge(n,3n)^{70}Ge, ^{70}Ge(n,2n)^{69}Ge, ^{74}Ge(n,4n)^{71}Ge, ^{70}Ge(n,p)^{69}Ge, ^{70}Ge(n,p)^{71}Ge, ^{72}Ge(n,p)^{73}Ge and ^{74}Ge(n,p)^{70}Ge.

The difference in atomic number Z between Si (14) and Ge (32) can explain such quantitative results, in so far as the number of nuclear reactions increases monotonically with Z, in particular inelastic and nonelastic interactions [5], as precisely reported in Table 2.

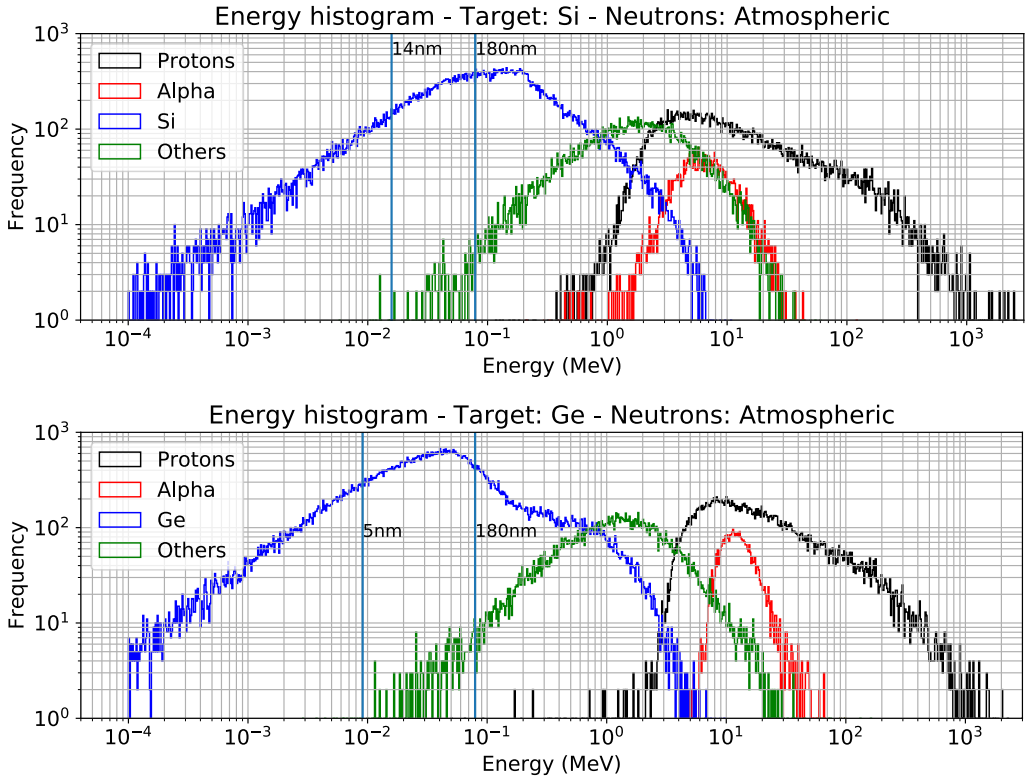

Figure 1. Energy histograms (1000 bins) of protons, alphas, target nucleus recoils and other ions produced by atmospheric neutron interactions in natural silicon and germanium bulk targets (1cm^2 × 20 µm, 5×10^8 n). The vertical lines labeled “5 nm” and “180 nm” indicate the minimum energies for these two technological nodes below which secondaries are not able to deposit a sufficient electrical charge needed to upset a SRAM memory cell.

Concerning now the total number of secondaries produced, Table 3 gives the distributions for the two material targets. We distinguished four categories of secondaries: recoil nuclei, protons + deuterons + tritons, helium nuclei (α + ^{3}He + ^{6}He) and finally a last category regrouping all the other ions produced. Logically with respect to results of Table 2, Ge exhibits much more secondaries than Si, about +33%. In details now, a

roughly similar number of protons, alpha particles and heavy ions are obtained in both materials, the main difference comes from the number of recoils which is much larger (+46%) in the case of Ge with respect to Si. This result is important in the perspective of device integration, since heavy recoil nuclei are characterized by low kinetic energies, intermediate or high LETs and extremely low ranges in target materials. This aspect is illustrated by the distribution histograms of secondaries in energy, LET and range, shown in Figures 1, 2 and 3 respectively. Below typically 0.1 MeV in energy and 10 nm in range, distributions are dominated by such recoil nuclei. The consequence is that they are only susceptible to induce weak amounts of electrical charge in the semiconductor material, not enough to induce SEEs in submicron technologies but possibly enough in nanometer ones, as discussed in the following. Another point shown by Figs. 1 to 3 is the notable difference for alpha particles produced in Si and Ge: their energy distribution is sharper for Ge with respect to Si and slightly shifted toward higher energies (maximum of the peak around 6 MeV for Si and above 10 MeV for Ge). For protons and other nuclei, similar distributions and energy domains are obtained (from 10^{-1} to 10^{3} MeV for protons, from 10^{-2} to a few tens of MeV for other nuclei) for the two targets, even if the proton distribution peak is around 10 MeV for Ge and only 4-5 MeV for Si. This slight differences in particle energy distributions are counterbalanced by a higher material density for Ge as compared to Si (Table 1). As a result, proton and alpha particles have the same range domains in both Si and Ge; for recoils and other ions, range distributions are marginally shifted towards smaller values for Ge as compared to Si. We examine in the following all the consequences of these distributions for both Si-based and Ge-based electronics reliability subjected to atmospheric neutrons.

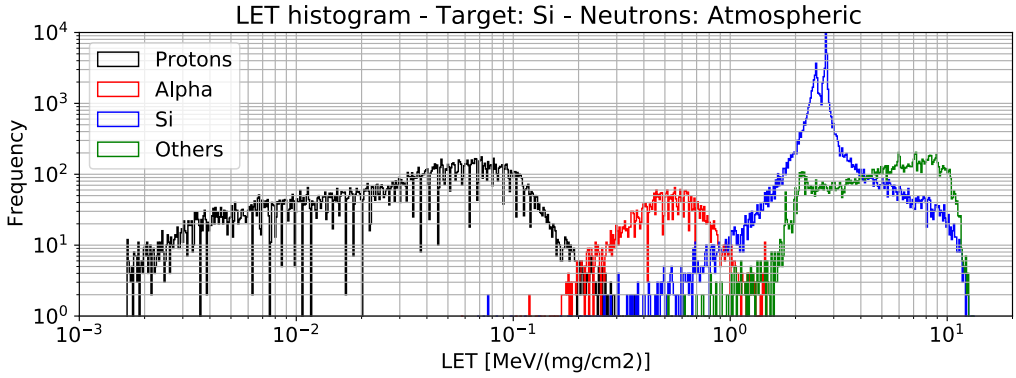

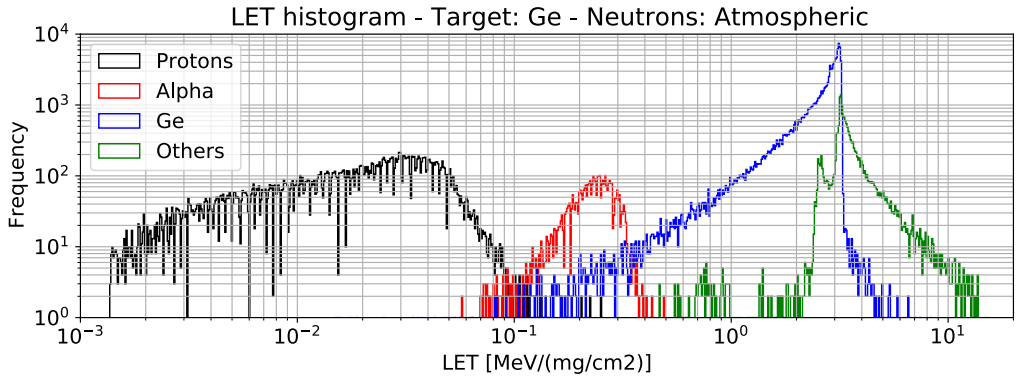

Figure 2. Initial LET histograms (1000 bins) of protons, alphas, target nucleus recoils and other ions produced by atmospheric neutron interactions in natural silicon and germanium bulk targets ($1cm^2 \times 20$ µm, 5×10^8 n).

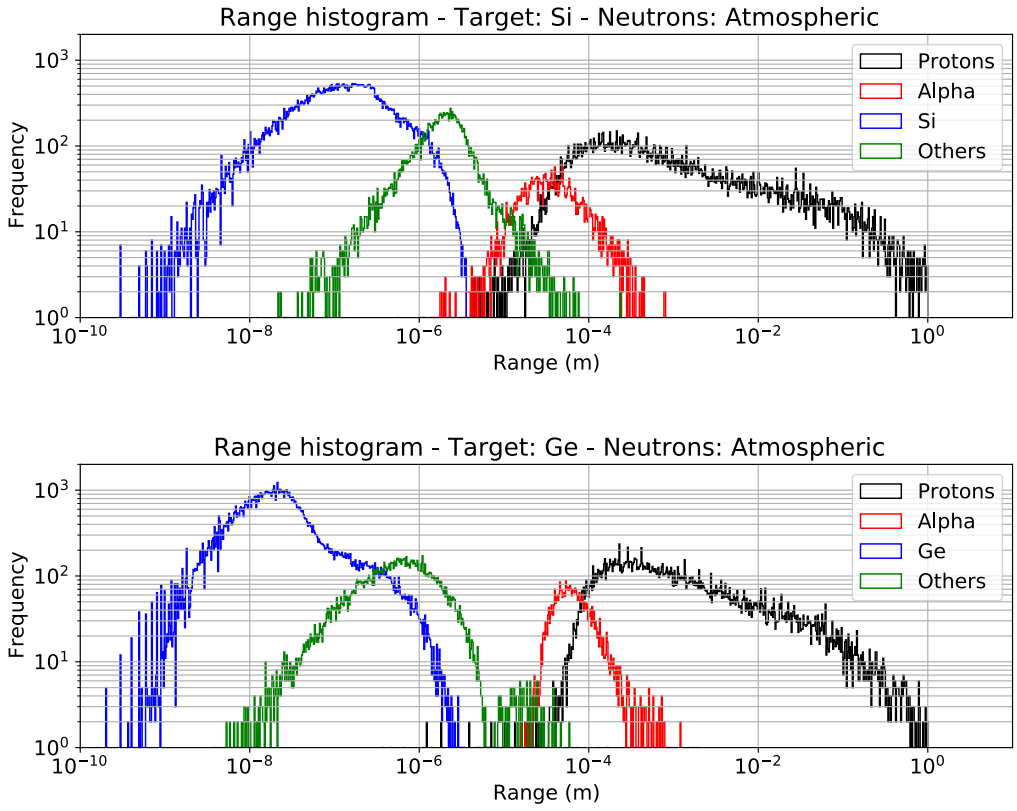

Figure 3. Range histograms (100 bins) of protons, alphas, target nucleus recoils and other ions produced by atmospheric neutron interactions in natural silicon and germanium bulk targets ($1cm^2 \times 20$ µm, 5×10^8 n).

4. Reliability concerns for Ge-based electronics

To quantify the impact of atmospheric neutrons on Ge-based electronics and its sensitivity to low energy secondary products, we considered the case of a SRAM memory and the evolution of its critical charge on a large domain of technological nodes, as shown in Figure 4. The critical charge Q_{crit} is a first-order metric that

has been introduced to evaluate the susceptibility for a static memory to be upset from a logical state to the other. It corresponds to the minimum amount of electrical charge that can flip the data bit stored in a memory cell.

For silicon devices, the evolution of Q_{crit} for technological nodes down to the "5 nm" node has been estimated from different sources, including experimental measurements, TCAD simulations and roadmap projections [21-24]. For germanium SRAMs, Q_{crit} values have been estimated from Si-based values considering both carrier mobility enhancement and semiconductor dielectric constant increase (see Table 1 for values). All these parameter variations contribute to reinforce transistor performances, in particular the maximum on-state current [16], and the capacitance of the struck node via the contribution of the different drain junction capacitances [25]. These variations tend to increase Q_{crit}, according to [26]. As obtained in our previous work [16] for a 0.18 µm bulk SRAM, Q_{crit} was found +25% higher for Ge-based devices as compared to the reference case of Si-based circuits. In the following, we consider such an increase of +25% for all values of Q_{crit} related to Ge-SRAM with respect to Si-SRAM cells.

To deposit an amount of electrical charge corresponding to Q_{crit} in a given semiconductor material, a secondary product must have a minimum energy $E_{min} = (Q_{crit}/q) \times E_{eh}$ where q is the electron elementary charge and E_{eh} is the average energy for creation of an electron- hole pair (eV). E_{eh} = 3.6 eV in bulk silicon and E_{eh} = 2.9 eV in bulk germanium. Each value of Q_{crit} in Figure 4 can thus be converted into a minimum energy threshold for both Si-based or Ge-based circuits. For a given product of energy E, a "necessary but not sufficient condition" to upset a memory bit is to verify $E > E_{min}$. On this basis, we can evaluate the number of interactions capable of producing at least one secondary product satisfying this condition, by post-processing Geant4 datafiles with such a "filter". Note that in this approach, the possible coupling of energy deposited by several secondary products is neglected. Results are shown in Figure 5 for both Si and Ge. For the 180 nm technological node characterized by the highest Q_{crit} value, the number of interactions verifying the previous condition is minimal: 53,566 for Si and 61,662 for Ge. On the contrary, for the most advanced node (5 nm), these numbers are much more important, due to the contribution of additional interactions: 80,457 for Si (+50%) and 105,353 for Ge (+71%). These additional interactions produce low energetic secondaries that have been identified to be exclusively recoil nuclei corresponding to the less energetic elastic interactions.

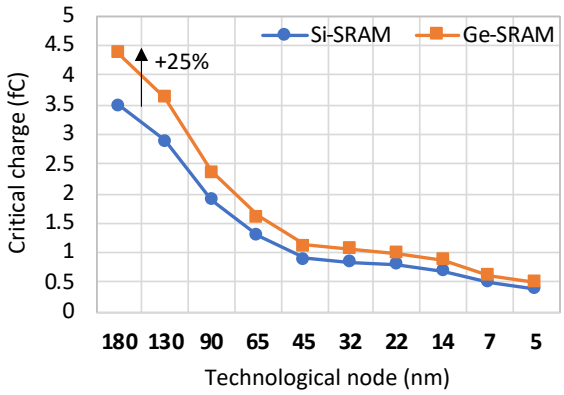

Figure 4. Critical charge versus CMOS technological nodes. After Refs. [21-24].

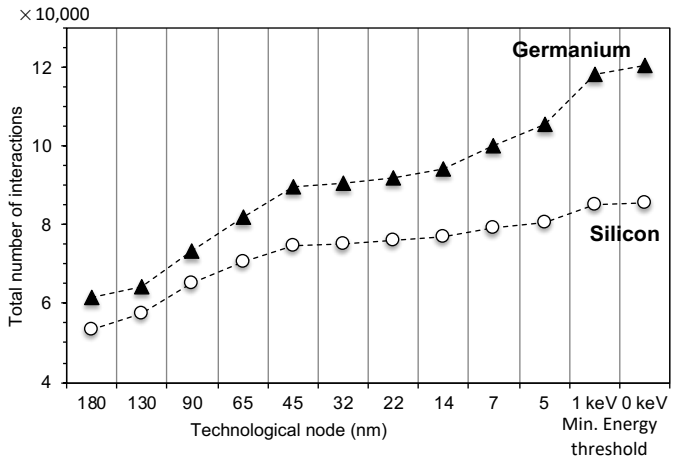

Figure 5. Total number of n-Si or n-Ge interactions that produce at least one secondary product satisfying the condition $E > E_{min}$ determined by Q_{crit} values of Figure 3 for technological nodes ranging from 180 to 5 nm. Two additional values are examined: E_{min} = 1 keV and 0 keV (no product filtering).

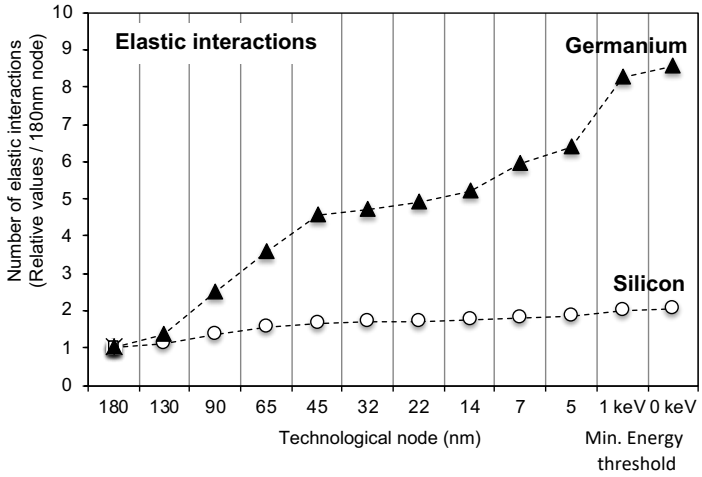

Figure 6. Relative evolution of the total number of elastic interactions that produce a recoil nuclei satisfying the condition $E > E_{min}$. Values are normalized with respect to the ones corresponding to the 180 nm node.

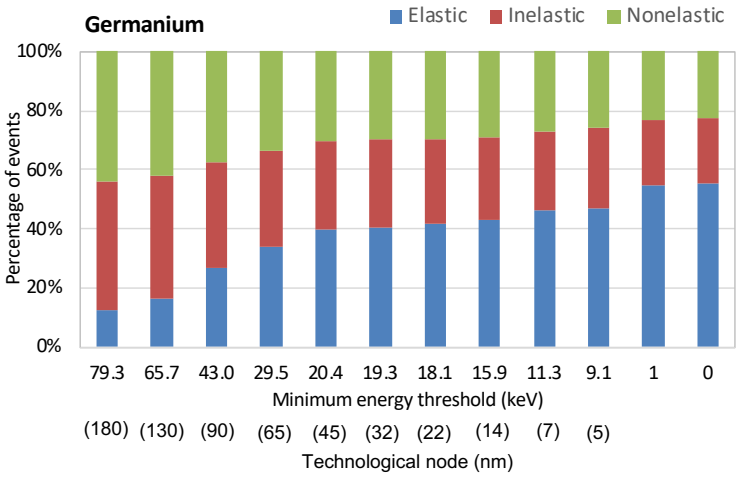

Figure 7. Proportions of elastic, inelastic and nonelastic events calculated for germanium on the basis of interactions that produce a recoil nucleus satisfying the condition $E > E_{min}$.

Figure 6 shows the relative evolution of this total number of elastic interactions that produce a recoil nucleus satisfying the condition $E > E_{min}$. Values have been normalized with respect to the ones corresponding to the 180 nm node. These result show that, for Ge, six times more reactions should be counted for the 5 nm node compared to the 180 nm one. For Si, this factor is only 1.8. This additional number of interactions to be considered for the most advanced nodes profoundly modify the proportions of elastic, inelastic and nonelastic events, as illustrated in Figure 7. Elastic events count for only 13% of the total number of events at 180 nm while it represents quasi the half of the events (46%) at 5 nm. Note that results of Figure 6 are in perfect agreement with our previous work in which we adopted a higher energy threshold (59 keV) [12].

Results from Figs. 5 to 7 correspond to a "necessary but not sufficient condition" for obtaining a SRAM upset since this criterion corresponds to a deposited charge and not a collected charge at the sensitive drains of the memory array. The next step of our analysis should be to couple the n-Si and n-Ge Geant4 databases to a soft error rate (SER) simulation code, also considering all the pertinent geometrical, technological and physical parameters for the envisaged technological nodes. This is clearly a complex task because: i) transistor architectures vary, typically above and below 20 nm, moving from a bulk to a FinFET architecture, ii) SRAM cell layouts also change when changing elementary device structure, iii) transport parameters of Si and Ge become size-dependent at nanometer scale (semiconductor properties, carrier confinement quantum effects, mobility reduction, etc.).

In the present study and in order to obtain first-order estimations for future Ge-SRAMs, we adopt the following simplified approach: Geant4 databases and SRIM files have been introduced in our TIARA Monte

Carlo simulation code [26] and SRAM arrays have been simulated for three nodes, i.e. 180 nm, 65 nm and 40 nm for which simulations have been previously validated with SER measurements obtained on silicon devices (for the reasons we have just mentioned, it does not seem reasonable to perform simulations for the following nodes for which we do not have at least an experimental point of comparison for silicon devices). To simulate Ge-SRAM, we used the same SRAM geometry cells and the same logical pattern as for Si and considered the Q_{crit} values reported in Fig. 4. We also changed in the code core the last five physical and electrical parameters given in Table 1. These parameter values are used to evaluate, for each semiconductor, the number of created electron-holes pairs, the carrier diffusion coefficients and the collection velocities at the drain contact level for minority carriers in both types of devices. Once parsing the Geant4 database for Ge with the corresponding SRIM data to obtain proper LET and ranges values in bulk Ge, TIARA computed the SER for a 20×20 cell array from the diffusion-collection model and direct impact model described in [27].

Table 4. Neutron SER numerical estimations for three generations of SRAM integrated on silicon using the Monte Carlo TIARA SER simulation code. For Si-based SRAMs, SER values have validated by real-time experiments for the three nodes [28-31]. The percentage of multiple cell upsets (MCU) is also reported.

		Silicon devices [28,29,30,31]			Projections for Ge devices		
Technological node (nm)	Cell area (μm^2)	Q_{crit} (fC)	n-SER (FIT/Mbit)	MCU events (%)	Q_{crit} (fC)	n-SER (FIT/Mbit)	MCU events (%)
130	2.5	3.2	420	7	4.0	204	18
65	0.62	1.8	260	28	2.24	142	25
40	0.30	0.9	486	46	1.13	400	44

Tables 4 report neutron SER numerical estimations for three generations of circuits, respectively for both Si-based and Ge-based SRAMs. These results show that the neutron soft error rate (n-SER) for Ge-devices is found lower than the n-SER of Si-devices for the three simulated nodes. The difference between the two series of values is within a maximum of factor 2 for 130 and 65 nm circuits, the difference is reduced to 20% for 40 nm SRAMs, which is not necessarily significant if we consider the uncertainties of the calculation and the absence of calibration on experimental data for Ge-circuits. Note that the percentage of multiple cell upsets (MCU) in the number of events is surprisingly higher for the 130 nm Ge-SRAM as compared to the value obtained for Si-SRAMs, certainly because the relative weight of nonelastic events (responsible of these events) is much more important at this node (Fig. 7), due to the elimination of low energy products, a direct consequence of a high Q_{crit} value for Ge-devices at this node.

Results of Table 4 confirm our very first conclusions [16], namely that the radiation response of Ge-based SRAM should be roughly like the one observed for Si-SRAM. The benefits of higher mobilities at circuit level (robustness of the memory cell) combined with a higher material density (slightly shorter product

ranges) seem to offset the negative impact of the relatively low energy value for electron-pair creation on transient current pulse magnitudes cumulated with a higher number of reactions and products produced by atmospheric neutrons. The balance between these opposite effects on the SER seems to be relatively equilibrated at this level of our investigations and, globally, SER values of Ge-SRAMs are clearly in the same order of magnitude than the ones related to Si-SRAMs for these three considered nodes. The additional contribution to the SER of very low energy products, significant for Ge material (Figs. 6 and 7), is not clearly evidenced at this scale of integration, which will need an important work to be properly simulated below 20 nm with new device and circuit architectures. At this level of our investigation, it remains a hypothesis to be confirmed.

5. Conclusion

In conclusion, this study showed that atmospheric neutrons induce much more interactions in germanium than in silicon for the same target geometry and neutron flux. In particular, the number of recoil nuclei is much larger in the case of Ge with respect to Si. Since they are characterized by low kinetic energies and extremely low ranges, their relative importance may increase when pushing device integration: they potentially appear as a new category of particles that expands the variety and spectrum of particles to which a nanometer circuit is sensitive. For ultimate CMOS nodes and in addition to the possible contribution of atmospheric muons and protons [32], very low energy elastic recoils induced by neutrons may thus have a significant impact of the circuit SER, primarily depending on the nature of the considered semiconductor material. If such an increase is found relatively moderate for silicon (+40%), the impact may be much more important for Ge-based circuits for which our results evidence a possible ×2 increasing factor when considering a scaling reduction from 180 nm to 5 nm nodes. Before envisaging SER simulation at ultimate CMOS nodes, we performed first soft error rate projections for germanium SRAMs in 130, 65 and 40 nm based on a simulation methodology previously developed and fully validated on silicon memories. These first estimations suggest that, at this scale of circuit integration, SER of Ge-SRAMs are in the same order of magnitude than the ones related to Si-SRAMs, the balance between negative and positive impacts of material parameters being relatively equilibrated. An important simulation work, currently in progress, is needed to investigate the radiation response of Ge-SRAMs at nanometer scale and to confirm or not the assumption of this study at material level highlighting the possible role of low energy products on the circuit SER.

References

[1] D.P. Brunco, B. De Jaeger, G. Eneman, A. Satta, V. Terzieva, L. Souriau, F.E. Leys, G. Pourtois, M. Houssa, K. Opsomer, “Germanium: The Past and Possibly a Future Material for Microelectronics”, ECS Transactions, Vol. 11, pp. 479-493, 2007.

[2] P.S. Goley, M. K. Hudait, “Germanium Based Field-Effect Transistors: Challenges and Opportunities”,

Materials, Vol. 7, pp. 2301-2339, 2014.

[3] M. Heyns, W. Tsai, “Ultimate Scaling of CMOS Logic Devices with Ge and III–V Materials”, *MRS Bulletin,* Vol. *34*, N°7, pp. 485-492, 2009.

[4] M. Moreau, D. Munteanu, J.L. Autran, F. Bellenger, J. Mitard, M. Houssa, “Investigation of capacitance-voltage characteristics in Ge /high-k MOS devices”, Journal of Non-Crystalline Solids, Vol. 355, no. 18-21, p. 1171-1175, 2009.

[5] H. Wu, N. Conrad, Wei Luo, P. D. Ye, "First experimental demonstration of Ge CMOS circuits," 2014 IEEE International Electron Devices Meeting, pp. 9.3.1-9.3.4, 2014.

[6] I.G. Neizvestny, “Germanium-based metal-insulator-semiconductor transistors as a direction for the further development of CMOS technology”. Optoelectron. Instrument. Proc., vol. 52, pp. 421–427, 2016.

[7] V. P. Hu, M. Fan, P. Su, C. Chuang, "Device design and analysis of logic circuits and SRAMs for Germanium FinFETs on SOI and bulk substrates," International Symposium on Quality Electronic Design, pp. 347-352, 2013.

[8] A. Toriumi A, T. Nishimura, “Germanium CMOS potential from material and process perspectives: Be more positive about germanium”, Japanese Journal of Applied Physics, vol. 57, pp. 010101, 2018.

[9] K.C. Saraswat, C.O. Chui, D. Kim, T. Krishnamohan, A. Pethe, “High Mobility Materials and Novel Device Structures for High Performance Nanoscale MOSFETs”, IEDM Techn. Digest 1-4, 2006.

[10] K.C. Saraswat, D. Kim, T. Krishnamohan, D. Kuzum, A.K. Okyay, A. Pethe, H.Y. Yu, “Germanium for High Performance MOSFETs and Optical Interconnects”, ECS Transactions, 16 (10) 3-12, 2008.

[11] P. Ye, T. Ernst, M. V. Khare, "The last silicon transistor: Nanosheet devices could be the final evolutionary step for Moore's Law," IEEE Spectrum, vol. 56, no. 8, pp. 30-35, 2019.

[12] D. Munteanu, J.L. Autran, “Susceptibility of Group-IV and III-V Semiconductor-based Electronics to Atmospheric Neutrons Explored by Geant4 Numerical Simulations”, in Numerical Simulations in Engineering and Science, edited by Srinivas P. Rao, IntechOpen, Chapter 7, 234, 2017.

[13] J.L. Autran, S. Serre, S. Semikh, D. Munteanu, G. Gasiot, P. Roche, "Soft-Error Rate Induced by Thermal and Low Energy Neutrons in 40 nm SRAMs", IEEE Transactions on Nuclear Science, Vol. 59, no. 6, p. 2658 – 2665, 2012.

[14] S. Serre, S. Semikh, S. Uznanski, J.L. Autran, D. Munteanu, G. Gasiot, P. Roche, "Geant4 Analysis of n-Si Nuclear Reactions From Different Sources of Neutrons and Its Implication on Soft-Error Rate", IEEE Transactions on Nuclear Science, Vol. 59, no. 4, pp. 714-722, 2012.

[15] J.L. Autran and D. Munteanu, "Atmospheric Neutron Radiation Response of III–V Binary Compound Semiconductors," IEEE Transactions on Nuclear Science, vol. 67, no. 7, pp. 1428-1435, July 2020.

[16] S. Moindjie, D. Munteanu, J.L. Autran, “Modelling and simulation of SEU in bulk Si and Ge SRAM", Microelectronics Reliability, vol. 100, 113390, 2019.

[17] https://geant4-userdoc.web.cern.ch/UsersGuides/PhysicsReferenceManual/html/hadronic/index.html

[18] P. Goldhagen, “Cosmic-Ray Neutrons on the Ground and in the Atmosphere”, MRS Bulletin, vol. 28, no. 2, pp. 131-135, 2003.

[19] M.S. Gordon et al., “Measurement of the Flux and Energy Spectrum of Cosmic-Ray Induced Neutrons on the Ground,” IEEE Transactions on Nuclear Science, vol. 51, pp. 3427-3434, 2004.

[20] J.L. Autran, D. Munteanu, “Soft Errors: from particles to circuits”. Taylor & Francis/CRC Press, 2015.

[21] N. Seifert, S. Jahinuzzaman, J. Velamala, R. Ascazubi, N. Patel, B. Gill, J. Basile, J. Hicks, “Soft Error Rate Improvements in 14-nm Technology Featuring Second-Generation 3D Tri-Gate Transistors”, IEEE Transactions on Nuclear Science, vol. 62, no. 6, pp. 2570-2577, 2012.

[22] K. Ni et al., “Single-Event Transient Response of InGaAs MOSFETs,” in IEEE Transactions on Nuclear Science, vol. 61, no. 6, pp. 3550-3556, Dec. 2014.

[23] B. Narasimham, V. Chaudhary, M. Smith, L. Tsau, D. Ball and B. Bhuva, "Scaling Trends in the Soft Error Rate of SRAMs from Planar to 5-nm FinFET," *2021 IEEE International Reliability Physics Symposium (IRPS)*, 2021, pp. 1-5.

[24] International Roadmap of Devices and Systems (IRDS), More More, Update 2020, Available online: https://irds.ieee.org/images/files/pdf/2020/2020IRDS_MM.pdf

[25] A. Pavlov, M. Sachdev, “SRAM Cell Stability: Definition, Modeling and Testing”. In: CMOS SRAM Circuit Design and Parametric Test in Nano-Scaled Technologies. Frontiers In Electronic Testing, vol 40. Springer, Dordrecht, 2008.

[26] P. Roche, G. Gasiot, J.L. Autran, D. Munteanu, R.A. Reed, R.A. Weller, “Application of the TIARA Radiation Transport Tool to Single Event Effects Simulation," IEEE Transactions on Nuclear Science, 2014, Vol. 61, p. 1498-1500.

[27] J.L. Autran, S. Semikh, D. Munteanu, S. Serre, G. Gasiot, P. Roche, “Soft-Error Rate of Advanced SRAM Memories: Modeling and Monte Carlo Simulation”, in “Numerical Simulation - From Theory to Industry”, Edited by M. Andriychuk, (INTECH, Vienna, 2012), Chapter 15.

[28] J.L. Autran, P. Roche, J. Borel, C. Sudre, K. Castellani-Coulie, D. Munteanu, T. Parrassin, G. Gasiot, J.P. Schoellkopf, “Altitude SEE Test European Platform (ASTEP) and First Results in CMOS 130nm SRAM”, IEEE Transactions on Nuclear Science, 2007, Vol. 54, no. 4, p. 1002-1009.

[29] J.L. Autran, P. Roche, S. Sauze, G. Gasiot, D. Munteanu, P. Loaiza, M. Zampaolo, J. Borel, “Altitude and Underground Real-Time SER Characterization of CMOS 65nm SRAM”, IEEE Transactions on Nuclear Science, Vol. 56, 2009, Vol. 56, no. 4, p. 2258-2266.

[30] J.L. Autran, S. Serre, D. Munteanu, S. Martinie, S. Semikh, S. Sauze, S. Uznanski, G. Gasiot, L. Dugouyon, P. Roche, “Real-Time Soft-Error Testing of 40nm SRAMs”, International Reliability Physics Symposium (IRPS’2012), Anaheim, USA, April 15-19, 2012, 3C-5.

[31] J.L. Autran, D. Munteanu, S. Moindjie, T. Saad Saoud, S. Sauze, G. Gasiot, P. Roche, “ASTEP (2005-2015): Ten Years of Soft Error and Atmospheric Radiation Characterization on the Plateau de Bure," Microelectronics Reliability, 2015, Vol. 55, p. 1506-1511.

[32] P. Roche, J.L. Autran, G. Gasiot, D. Munteanu, “Technology downscaling worsening radiation effects in bulk: SOI to the rescue”, in: IEEE International Electron Device Meeting, IEDM, 2013, pp. 766–769.